Comparing Hydrogen and Jet-A for an N+3 Turbofan with Water Recirculation using Gradient-Based Optimization

Peter N. Atma*, Andrew H .R. Lamkin†, and Joaquim R. R. A. Martins‡
University of Michigan, Ann Arbor, MI, 48109

Advances in commercial propulsion technology led to the development of efficient high bypass ratio turbofan engines with larger overall pressure ratios and internal temperatures. Current trends suggest that geared ultra high bypass ratio turbofans are the next generation of commercial propulsion systems. Furthermore, the emphasis on decreasing emissions has driven the exploration of hydrogen-powered aircraft, adding to the already challenging design space. Carrying and burning hydrogen introduces complexity and weight penalties that we must offset using the fuel's thermodynamic and chemical properties. In this study, we create a closed-loop water recirculation system with a zero-dimensional thermodynamic model and compare the benefits between jet-A and hydrogen fuels. We perform a gradient-based optimization parameter sweep to explore the trade-offs between performance and emissions using both fuels with water recirculation. The results quantify the design space for next-generation propulsion concepts that can take advantage of hydrogen fuel's advantageous thermodynamic properties to reduce emissions and improve performance.

I. Introduction

The effects of climate change are pushing the aviation industry towards hydrogen-fueled propulsion systems as a solution to reduce emissions. N+3 technology estimates for turbofan engines that burn hydrocarbon fuels suggest that higher efficiency can be achieved by designing ultra high bypass ratio (UHBR) engines with small cores and high overall pressure ratios (OPR). Higher OPR and smaller cores challenge the limits of compressor and turbine design, placing an upper bound on potential performance and emissions improvements. Switching to hydrogen as the primary fuel source reduces carbon dioxide emissions immediately, but adds complexity and weight that offset the benefits. However, hydrogen is a versatile fuel with advantageous chemical and thermodynamic properties that can be exploited to increase the performance and reduce emissions. We introduce a closed-loop water recirculation model that demonstrates the possible efficiency gain when hydrogen is used for purposes other than combustion.

Water injection is the process of injecting water upstream of the combustor as finely atomized droplets. NASA, Boeing, and Rolls-Royce studied this concept and suggested that this technique reduces the NOx emissions as much as 47 percent [1]. Additionally, water injection improves fuel efficiency and thrust output with lower combustion temperatures that can improve the lifetime of turbine blades and reduce noise [1]. Traditional propulsion systems that burn hydrocarbon fuels would require external water storage on the aircraft for water injection [2]. The added weight of tanks, pumping, and ducting makes this concept infeasible for a conventional aircraft. The main product of hydrogen combustion is water vapor and can thus be recovered from the exhaust stream [3]. Condensing water vapor from the exhaust stream of hydrogen combustion and recirculating it elimiates the requirement for storage tanks. This allows for the theoretical design of a closed loop water feedback system inside the propulsion cycle. Indeed, the aerospace industry is starting to look into this technology to make hydrogen-powered aircraft economical *.

Zero-dimensional cycle modeling is an efficient tool for predicting the initial design, performance, and emissions of new propulsion concepts. Zero-dimensional analysis uses a first-principles approach with a chemical equilibrium analysis (CEA) thermodynamics solver [4] that considers the molecular species of different fuels. The industry standard for thermodynamic cycle analysis is the Numerical Propulsion System Simulation (NPSS) framework [5]. NPSS is a modular object-oriented library that models engine components as individual blocks with several thermodynamic solvers. Hendricks and Gray [6] created a new tool called pyCycle with the same functionality as NPSS with analytical derivatives for each engine component and thermodynamic solver [7]. pyCycle is built on top of the OpenMDAO

*MSE Student, Department of Aerospace Engineering, AIAA Student Member
†Ph.D. Candidate, Department of Aerospace Engineering, AIAA Student Member
‡Professor, Department of Aerospace Engineering, AIAA Fellow
*https://arpa-e.energy.gov/technologies/projects/hydrogen-steam-and-inter-cooled-turbine-engine-hysite

framework [8] to enable gradient-based optimization and leverage hierarchical nonlinear solver structures for robustness. OpenMDAO provides a framework for computing coupled derivatives efficiently using the modular analysis and unified derivatives (MAUD) architecture which supports a large number of design variables [9].

In this work, we analyze the thermodynamic benefits of a closed-loop water vapor recovery and water injection system in a high-bypass turbofan engine. We develop pyCycle components for water injection and vapor recovery to quantify the benefit of a closed loop recirculation system. We use gradient-based optimization to minimize fuel burn subject to performance requirements using both jet-A and hydrogen at a range of flight conditions. The optimized results show the trade-off between complexity, performance, and efficiency for jet-A and hydrogen fuels.

This work is organized as follows. First, in Section II, we introduce the turbofan model and explain the water injection and water recovery components. In section III the implementation of the multipoint optimization problem is discussed. Finally, we present the optimized results and discuss the design space in section IV.

II. Methodology

The UHB turbofan model is the NASA advanced technology "N+3" engine [10]. The N+3 reference cycle represents a UHB ratio geared turbofan that could be available in the 2030 to 2040 time frame. The flow path consists of an inlet that directs ambient air through a fan, followed by a duct that splits the flow into a core and a bypass stream, each ending in a core and bypass nozzle, respectively. The low pressure system is split into two mechanical subsystems. First, the fan is connected to the gearbox that reduces the shaft speed to decrease the fan tip speeds. Second, the gearbox attaches to the low-pressure shaft that connects to the low-pressure compressor (LPC) and low-pressure turbine (LPT). The high pressure compressor (HPC) is connected to the high pressure turbine (HPT) by the high pressure shaft.

We introduce the closed-loop water recovery system as a feedback loop that transports water from the exhaust to upstream of the compressors. The recovery system injects vaporized water into the core stream that reduces the combustion temperature due to heat absorption. The vapor recovery component is placed directly before the core nozzle to extract water from the exhaust and recycle it back to the injector.

In this section we present the full engine layout and provide details on the multipoint zero-dimensional modeling approach. We explain the implementation and assumptions of the water recovery model and the coupling with the thermodynamic cycle.

A. Propulsion Model

The N+3 model is implemented in pyCycle [6], a zero-dimensional thermodynamic cycle modeling library with analytical gradients. Zero-dimensional models are a collection of components that combine to form a unified thermodynamic cycle. The N+3 UHB geared turbofan model consists of twenty-five different elements that define the flow path and the mechanical systems. Thermodynamic quantities are solved and exchanged using CEA at flow path boundaries represented by black arrows between blue flow path components in Figure 1. The fan, gearbox, low pressure, and high pressure systems are connected by three mechanical shafts depicted in red in Figure 1.

We impose *balance* equations on the cycle to satisfy the physical governing equations, conservation laws, and design rules. *Balance* relationships are formulated as equations in the form $r(u) = 0$ where r is a residual function and u is an implicit state variable. We use Newton based solvers to find the value of the state variables that drive the set of balance residuals to zero. Hendricks and Gray provide the balance equations for the N+3 engine model and further detail the cycle setup.

B. Water Recovery Model

We implemented the closed-loop water recovery system as a feedback system that extracts water from the exhaust stream and injects it upstream of the HPC. We chose this injection location based on claims from a study by NASA, Boeing, and Rolls-Royce [1] that water injection directly into the combustor is unnecessary. The water vapor recovery component sits downstream of the LPT and extracts water from the flow before it exits the core nozzle. In the model of the extractor, we are assuming that a fraction of the total water available in the exhaust stream is recovered and that there are no pressure or temperature losses associated with this process. The component flow interface and mechanical connections, including the water injector and water extractor, are depicted in Figure 2.

To account for the humidity of the inlet air as well as the increased humidity after water injection, we modified the composition of the air mixture upstream of the combustor. pyCycle provides a `wet-air` dataset that introduces H_2O molecules to the composition of air. We prescribe atmospheric mass-specific humidity as a water-to-air ratio (WAR)

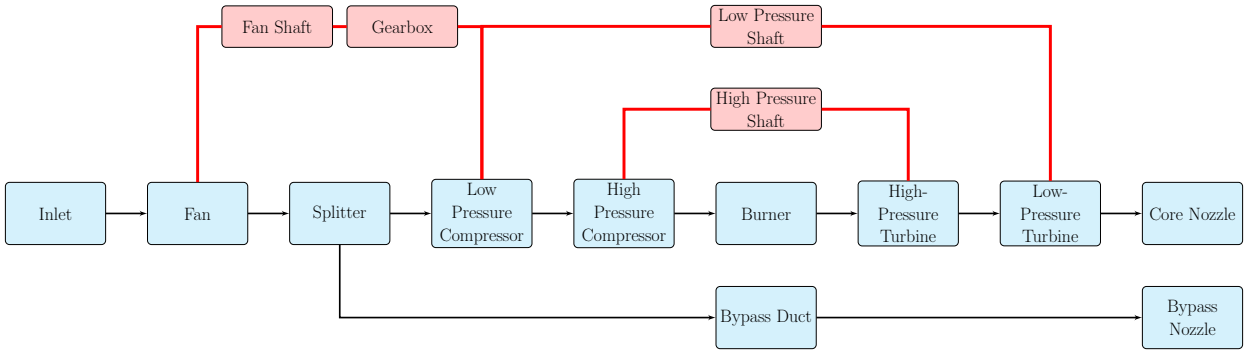

Fig. 1 Simplified layout of the N+3 engine cycle, adapted from Hendricks and Gray [6]. Black arrows are flow connections, red lines are mechanical connections, blue boxes are cycle elements, red boxes are shaft elements.

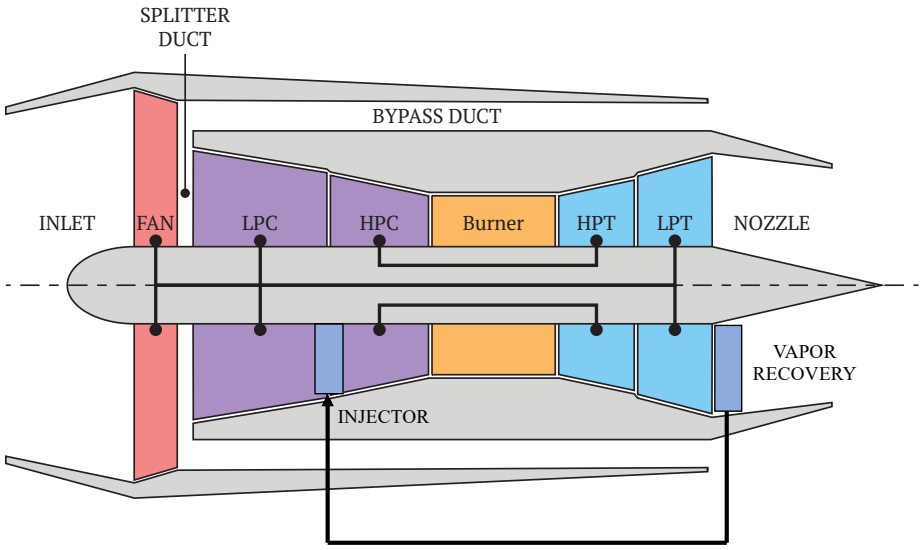

Fig. 2 The configuration of a high-bypass turbofan model with an integrated closed-loop water vapor recovery and injection system. The water vapor recovery system (extractor) extracts a fraction of the water in the core stream and reinjects it upstream of the high-pressure compressor. This diagram illustrates the feedback effect that this implementation has on the overall core flow.

that is defined as the ratio of H_2O to air in the reactants of the inflow mixture. Kalnay et al. [11] give the humidity values for each flight condition.

We introduce two new thermodynamic models for water recirculation in pyCycle. A water injector adds water to the flow upstream of the HPC, while a water extractor diverts a portion of the water in the flow away from the exhaust stream. The injector operates similarly to fuel injection in the pyCycle combustor component. We determine a WAR that is analogous to the fuel-to-air (FAR) ratio in the combustor. This WAR is used to compute the chemical species present in the flow at the current thermodynamic state, determined by the incoming flow. The new species composition and thermodynamic state are determined using the pyCycle CEA solver [7]. The water injector inputs are the mass flow rate and mass fraction of water. We can solve for the mass flow rate on a mixture basis using the WAR, or directly by specifying the mass flow rate of water. A schematic of the injector is shown in Figure 3 where Y_{H_2O} is the mole fraction of water molecules.

The water extractor model diverts a fraction of a specific species from one flow path to another. The CEA solver calculates the inflow composition and the extractor separates a specific species based on a mass fraction input. The composition of the core stream is updated to represent the remaining mixture after the extractor model removes the

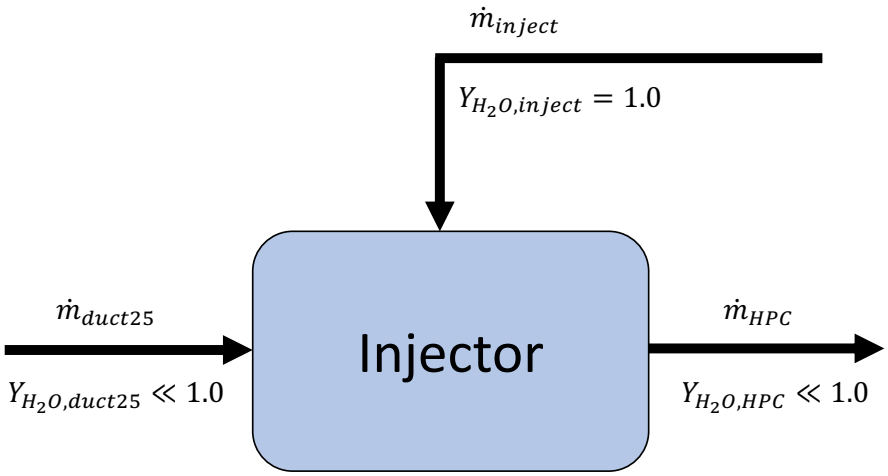

Fig. 3 Injector component schematic. Water from the extractor is simply injected into the core flow upstream of the high-pressure compressor.

desired species from the incoming flow. We then solve for the thermodynamic state and flow path areas at the outflow of both extractor streams. A simple schematic of the extractor is shown in Figure 4 where Y_{H_2O} is the mole fraction of water molecules and $X_{H_2O,k}$ is the fraction of water that is recovered from the core stream.

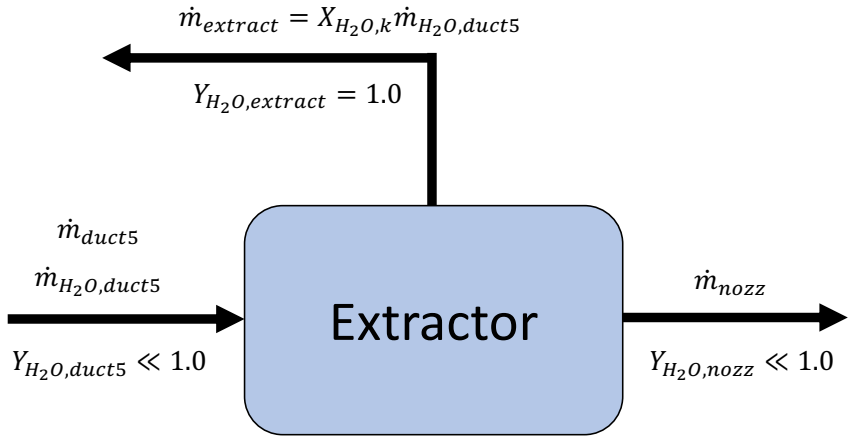

Fig. 4 Extractor component schematic. A certain mole fraction of the flow coming out of duct5 is comprised of water of which a certain specified fraction is extracted. The extracted water is routed back upstream to the injector and the rest is simply exhausted out the nozzle.

We connect one outflow stream of the extractor to the inflow stream of the injector to complete the water recirculation system. The model results in a mismatch between the mass flow rate upstream of the HPC and the mass flow rate exiting the core nozzle. To preserve conservation of mass, we treat the water recirculation as a nonlinear cycle that must converge before the engine calculation is physically balanced. In this model, we are assuming the water molelues are removed from the exhaust stream with no pressure or temperature losses. Additionlly, the model assumes the injected water molecules are at the same pressure and temperature as the air flow just before the HPC. Therefore, we are capturing the effect of adding pure water to the stream since zero-dimentional analysis cannot reproduce the effect of evaporation. We illustrate the water recirculation loop and the nonlinear solver connections in Figure 6.

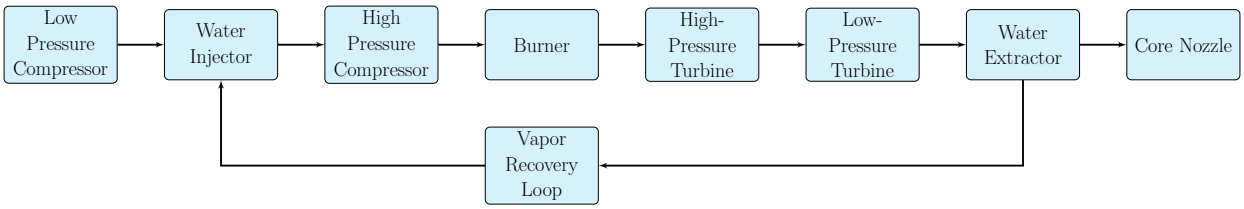

Fig. 5 Simplified layout of the N+3 engine cycle with the closed-loop vapor recovery. Black arrows are flow connections, red lines are mechanical connections, blue boxes are cycle elements, red boxes are shaft elements.

C. Multipoint Model

We operate the engine cycle in different modes depending on the desired conservation relationships, design rules, and flight conditions. In "on-design" mode, we prescribe important cycle inputs such as turbo machinery efficiencies, pressure ratios, and combustion temperatures. The "off-design" mode inherits the flow path areas and turbo machinery map scalars from the "on-design" analysis. We enforce design rules as balance equations between different design points to consider the performance of the engine cycle at limiting flight conditions. Table 1 shows the different altitudes and mach numbers at each flight condition.

The "on-design" point is top-of-climb (TOC) with "off-design" conditions at rolling takeoff (RTO), sea-level static (SLS), and cruise (CRZ). Each flight condition is either critical to the performance or limits the design of the engine.

The N+3 engine model has many complex thermodynamic and performance connections between the different operating conditions such as temperature ratios and cooling requirements. Therefore, the N+3 engine model computes the engine performance at the four different operating conditions in order to resolve these connections. The SLS operating condition is important for ensuring that the turbomachinery and flow paths are designed to a meet static thrust target. The RTO operating condition is important for specifying the upper limit of the combustor temperature and cooling requirements for a thrust target during take-off. The TOC operating condition is important for specifying the required thrust during the climb at the design altitude. Finally, the CRZ operation condition is important for specifying that the turbomachinery and flow paths are designed to meet cruise target thrust. To account for each of these operating conditions, the N+3 model uses a technique called Multipoint Design Point (MDP) modeling to converge the model to an engine design. This final design must satisfies the requirements at each of these operating conditions. The altitude and mach number of each of the operating conditions is shown in Table 1.

Table 1 Altitude and mach numbers at each of the flight conditions considered in the multipoint formulation.

Parameter	TOC	RTO	SLS	CRZ	Units
Altitude	35000	0	0	35000	ft
Mach	0.8	0.25	0.0	0.8	-
Humidity Ratio	0.00017	0.009	0.009	0.00017	kg/kg

The TOC point is the "on-design" condition since it is desireable to specify combustor temperatures and pressure ratios at this point. The design point for the model sets all of the engine sizing such as areas and pressure ratios across components. The off-design points inherit the size of the engine in terms of the cross-sectional areas from the design point but operate at the corresponding required thrust, cooling, and environmental conditions.

We size the water recovery system at the cruise condition because it is the longest and most important phase of flight for fuel burn reduction. To size the areas of the injector and extractor at CRZ, we only connect the thermodynamic state variables across these components at the corresponding operating condition and set the areas of both components at the CRZ point. These connections are shown graphically in the XDSM diagram in Figure 6.

The N+3 multipoint model has many constraints on the model that set conservation and design values using *balance* components. A Newton solver is used to converge these conservation an design values such $r = 0$. The conservation *balance* residuals are associated with each of the three shafts at each design condition. The state variables that set the shaft conservation residuals are the turbomachinery pressure ratios (PR_{Fan}, PR_{LPC}, PR_{HPC}) at TOC and shaft speeds (N_{Fan}, N_{LPC}, N_{HPC}) and engine mass flow rate ($\dot{m}$) at the "off-design" points. The design constraints are also set using *balance* residuals. For the TOC point, T_4 is set by the fuel-to-air ratio (FAR) of the burner and OPR is

set by HPC_{PR}. Additionally, a constraint on the turbomachinery polytropic efficiency is set based on technological assumptions. These TOC balance residuals are summarized in Equation (1) [6].

$$r_{des} \rightarrow \begin{cases} T_{4,TOC} = T_{4,des} \\ OPR_{TOC} = OPR_{des} \\ \eta_{poly,i,TOC} = \eta_{poly,i,des} \end{cases} \tag{1}$$

The outputs for the TOC point based on these design constraints are TSFC and F_{net}. For the "off-design" points, the target fan stall margin is set by the bypass ratio (BPR) and target net thrust is mainly set by FAR. Additionally, the engine cooling mass flow rate residuals are set by cooling needs at RTO using a perscibed value. These "off-design" residuals are summarized in Equation (2) [6].

$$r_{od} \rightarrow \begin{cases} R_{Fan} = R_{Fan,target} \\ F_{net} = F_{net,target} \\ \dot{m}_{cooling,err,k} = 0 \end{cases} \tag{2}$$

Solving for all of the state and design variables while satisfying constraints could be accomplish with only an optimizer to simplify the problem. However, using a solver to converge constraints using *balance* components creates a reduced-space problem with few design variables for the optimizer. This increases the complexity of the multipoint nonlinear solution but simplifies the problem for the optimizer and is the preferred method in cycle analysis.

In the N+3 model implementation presented in the pyCycle paper, the bypass ratio (BPR) at TOC is computed using a *balance* component. The *balance* component for BPR_{TOC} uses the exit velocity ratio of the core and bypass nozzles which is given as:

$$V_{ratio} = \frac{V_{core,ideal} C_{v,core}}{V_{bypass,ideal} C_{v,bypass}} \tag{3}$$

where V_{ideal} is the exit velocity of a nozzle and C_v is the velocity coefficient of the nozzle which represents non-ideal effects. This adds a constraint where the core exit velocity is higher than the bypass exit velocity.

With all of the sub-models of the N3 engine presented, the complete engine cycle XDSM diagram is shown in Figure 6. This is the multidisciplinary design analysis block of the model.

III. Optimization Problem

We performed multipoint gradient-based design optimization of the N+3 engine model considering the TOC, RTO, SLS, and CRZ flight conditions. The objective is to minimize fuel burn subject to design and performance constraints at each flight condition.

For measuring the efficiency of jet engines, thrust-specific fuel consumption (TSFC) is used in cycle analysis since it represents how much fuel is burned at a given thrust level. However, when comparing Jet-A and hydrogen fuels this is not such a good metric since a given mass flow rate of hydrogen has an energy content almost 3 times that of Jet-A. A better metric for comparing the relative efficiencies of an engine running on Jet-A versus hydrogen is thrust-specific energy consumption (TSEC). TSEC is TSFC multipied by the lower heating value (LHV) of the fuel shown in Equation (5).

$$TSFC = \frac{\dot{m}_{fuel}}{F_{thrust}} \tag{4}$$

$$TSEC = \frac{\dot{m}_{fuel} LHV}{F_{thrust}} = TSFC \times LHV \tag{5}$$

Therefore, TSEC at the cruise condition is the objective function in the optimzation problem. An XDSM diagram of the optimization problem with the multipoint formulation is shown in Figure 7.

The TOC point constraints shown in Figure 7 are only the constraints imposed on the model at optimizer level.

The design variables for this problem are water recovery fraction at CRZ ($X_{H_2O,CRZ}$), fan pressure ratio ($PR_{fan,TOC}$), low pressure compressor pressure ratio ($PR_{LPC,TOC}$), overall pressure ratio at CRZ (OPR_{TOC}), burner temperature at RTO ($T_{4,RTO}$), TOC-RTO burner temperature ratio ($T_{4,ratio}$), and the nozzle velocity ratio at CRZ ($V_{ratio,CRZ}$). Only the

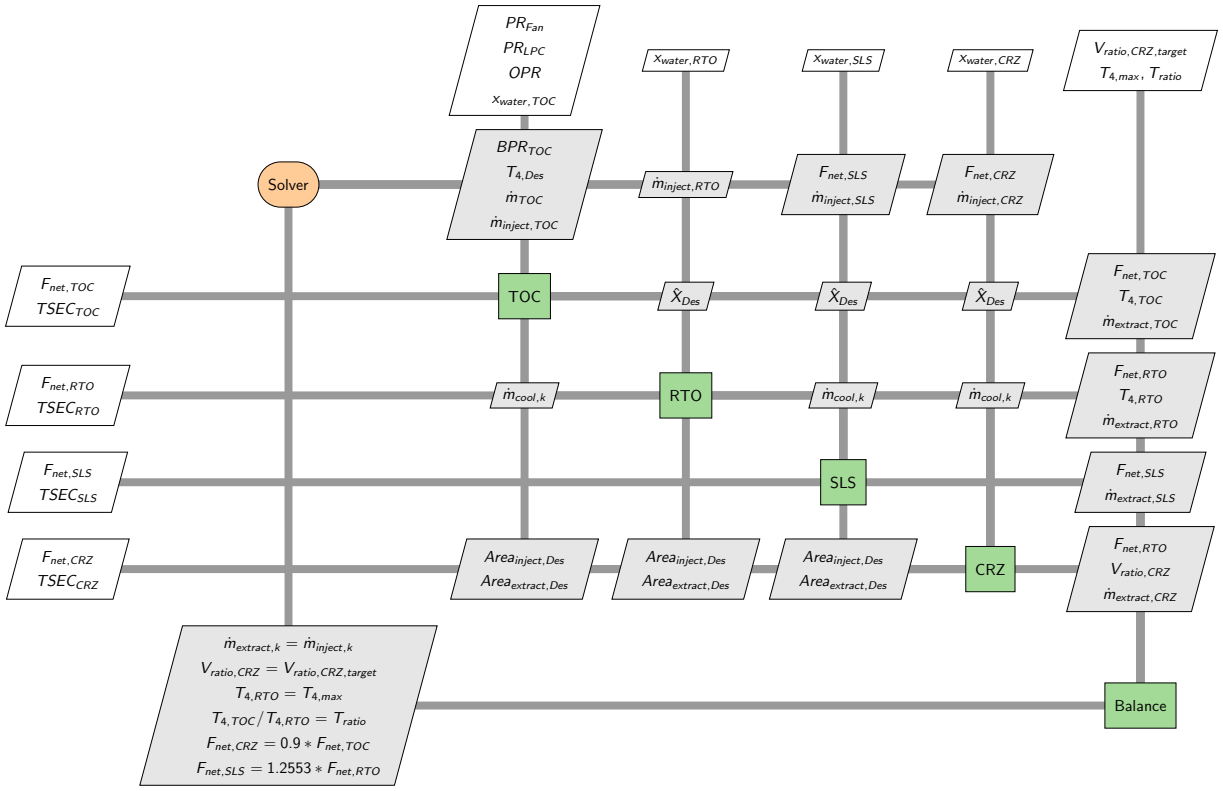

Fig. 6 Full multidisciplinary design analysis (MDA) model N+3 XDSM diagram. This XDSM diagram shows the multipoint coupling between the different operation conditions and shows how the water recovery fractions are used to solve for water mass flow rates.

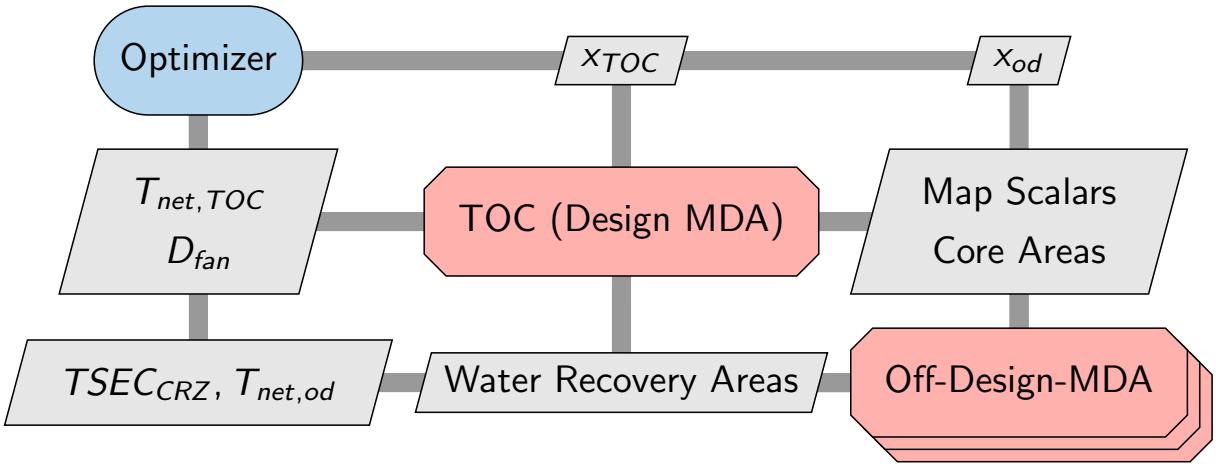

Fig. 7 XDSM diagram of the multipoint optimization problem with objective, constraints, and MDA block. The XDSM diagram shows the variables and outputs within the optimization model and how each of these values is connected to the optimizer and MDA block.

water recovery fraction at CRZ is a design variable since we are optimizing $TSEC_{\text{CRZ}}$. TOC-to-RTO burner temperature

ratio ($T_{4,\text{ratio}}$) is shown in Equation (6).

$$T_{4,\text{ratio}} = \frac{T_{4,\text{TOC}}}{T_{4,\text{RTO}}} \tag{6}$$

This optimization problem was run for both Jet-A and H2 fuels using the fuel properties in 2 and flight conditions in Table 1.

Table 2 N+3 model fuel properties. The lower heating values are given for each fuel used to compute TSEC.

Parameter	Value	Units	Description
LHV_{JetA}	18564.0	BTU/lbm	Lower heating value of Jet-A [†]
LHV_{H2}	51591.0	BTU/lbm	Lower heating value of H2 [‡]

The optimization problem objective function, design variables, and constraints are shown in Table 3 below.

Table 3 Multipoint optimization problem definition. The objective function is the thrust specific energy consumption at the cruise condition. The constraints are net thrust and engine diameter constraint at the design point, TOC.

	Variable/Function	Description	Units	Quantity
minimize	TSEC_{CRZ}	Thrust-specific energy consumption at CRZ (Equation (5))	lbm/s	1
with respect to	$X_{\text{H}_2\text{O,CRZ}}$	Water recovery fraction at CRZ	-	1
	$\text{PR}_{\text{fan,TOC}}$	TOC fan pressure ratio	-	1
	$\text{PR}_{\text{LPC,TOC}}$	TOC low-pressure compressor pressure ratio	-	1
	OPR_{TOC}	TOC overall pressure ratio	-	1
	$T_{4,\text{RTO}}$	RTO combustor temperature	°R	1
	$T_{4,\text{ratio}}$	TOC-to-RTO temperature ratio (Equation (6))	-	1
	$V_{\text{ratio,CRZ}}$	Core-to-bypass nozzle velocity ratio at CRZ (Equation (3))	-	1
		Total		7
subject to	$F_{\text{net,TOC}} \geq 5800.0$	Target net thrust at TOC	lbf	1
	$D_{\text{fan}} \leq 100$	Maximum Fan Diameter	inch^2	1
		Total		2

OpenMDAO [8] is a modular framework that enables multidisciplinary gradient-based optimization with analytic coupled derivatives. We use pyOptSparse [12] to facilitate the use of state-of-the-art optimization software through a unified python interface. We solve the optimization problem listed in Table 3 with SNOPT [13], a gradient-based sequential quadratic programming (SQP) algorithm for large-scale constrained problems.

IV. Results

Our fuel performance metric is TSEC but minimizing $\dot{m}_{fuel}$ is a better posed optimization problem since we will also have thrust constraints. Therefore, the fuel flow rate at CRZ, $\dot{m}_{fuel,CRZ}$, was set as the objective.

When $T_{4,\text{RTO}}$ and $X_{\text{H}_2\text{O,CRZ}}$ are design variables at the same time it was found that the optimizer pushes $T_{4,\text{RTO}}$ down and $X_{\text{H}_2\text{O,CRZ}}$ up. Since these two variables are at odds with each other and the upper limit for $X_{\text{H}_2\text{O,CRZ}}$ is where the model breaks, $T_{4,\text{RTO}}$ was set as the optimal value from the optimizations with no water recirulation. The upper bound on $X_{\text{H}_2\text{O,CRZ}}$ was found to be around 30% for Jet-A and 17% for H2.

The 4 optimizations mentioned in the section III were run and solved. The optimality, feasibility, and merit function for each optimization is shown plotted in Figure 8.

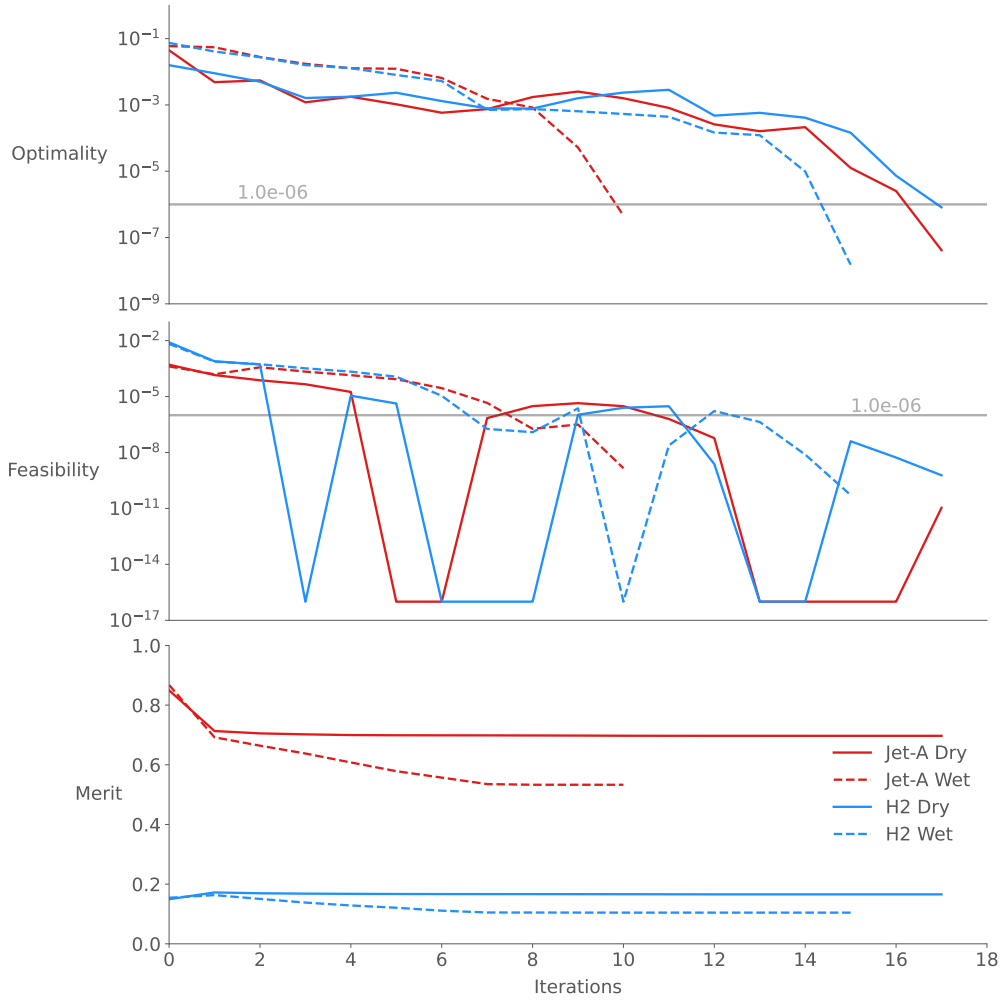

Fig. 8 The optimality, feasibility, and merit fuction history for each optimization problem. Jet-A without water recovery is shown with the solid lines, the Jet-A with water recovery is shown with dashed lines, hydrogen without water recovery is shown with dash-dot lines, and hydrogen with water recovery is shown with dotted lines.

From this plot we can visually check that each optimization achieved optimality and feasibility, and that the merit function reached a steady-state value. Indeed, we see quadratic convergence in the optimiality of the problem near the optimal solution as expected. The design variable history for each optmization problem is shown in Figure 9.

From this figure we see that the design variables start at the initial values and converge toward their optimal value. Note that the $T_{4,\mathrm{RTO}}$ variables are only present for the optimzations without water recovery and the $X_{\mathrm{H_2O,CRZ}}$ variables are present only for the optimizations with water recovery. The constraint history for each optmization problem is shown in Figure 10.

From this figure we can see that the constraints are quickly satisfied and for the most part remain feasible for the duration of the optimization. The resulting optimal values from the optimization problems are shown in Figure 11 on a parallel coordinate plot.

We can see that the resulting engine designs are all very similar. The main differences in the engine designs are the pressure ratios and temperatures. Between the two fuel types, the water recovery fraction for both is pushed up to the upper limit of the design space. Given that more water is present in the exhaust stream of the H2 engine, the H2 engine can recover a smaller fraction of the water compared to the Jet-A engine. The water recovery flow rates for the Jet-A and H2 engines was 0.324 lbm/s and 0.405 lbm/s, respectively. Therefore, the H2 has the benefit of being able to recover more water at a lower fraction of the overall core exhaust stream water. With water recovery, we see slightly higher pressure ratios across the fan and overall pressure ratio while the LPC pressure ratio is pushed to its technological

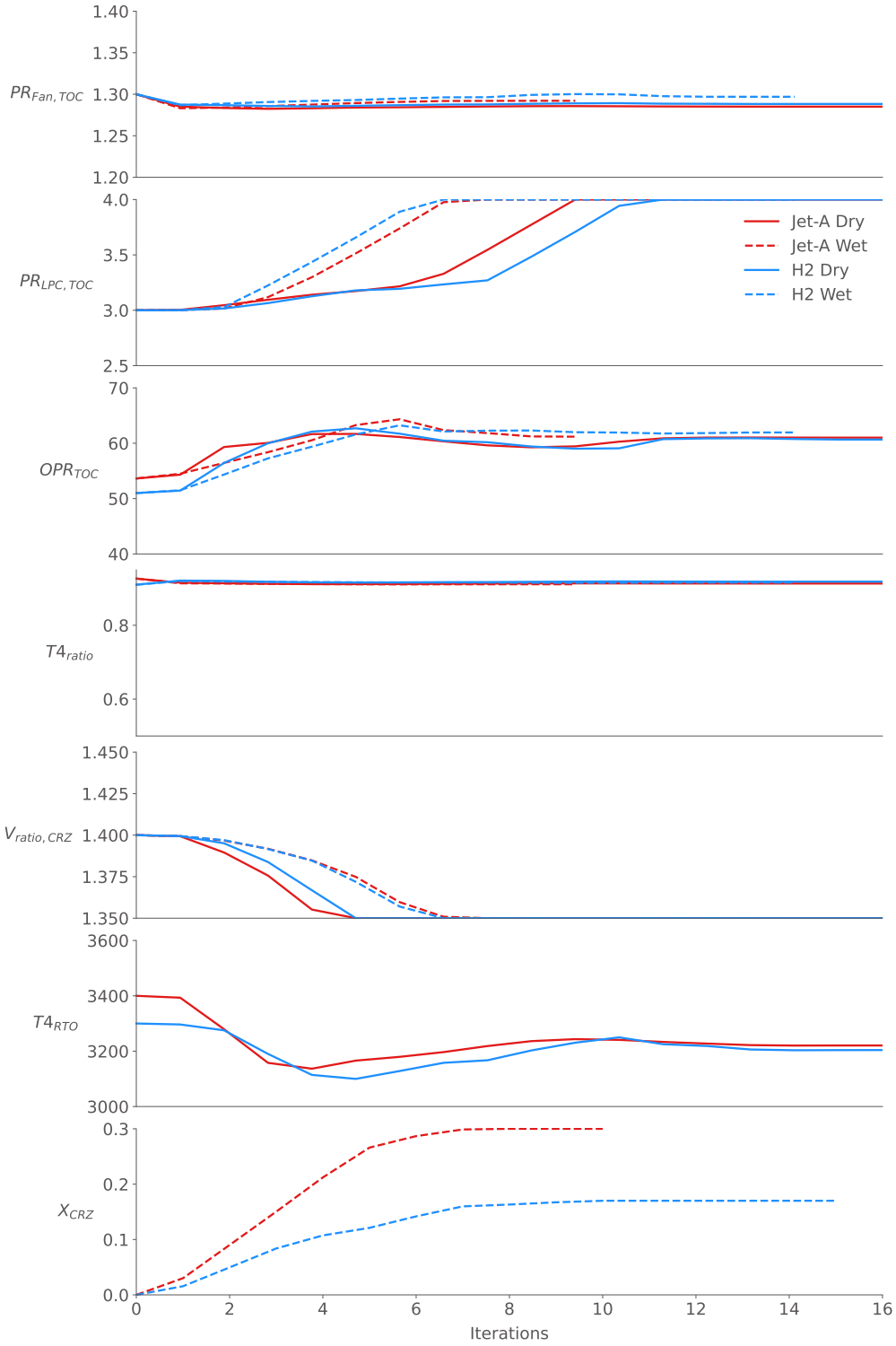

Fig. 9 The design variable history for each optimization problem. Jet-A without water recovery is shown with the solid lines, the Jet-A with water recovery is shown with dashed lines, hydrogen without water recovery is shown with dash-dot lines, and hydrogen with water recovery is shown with dotted lines.

upperbound. We only see differences in $T_{4,\mathrm{RTO}}$ without water recovery due to these values are fixed for water recovery.

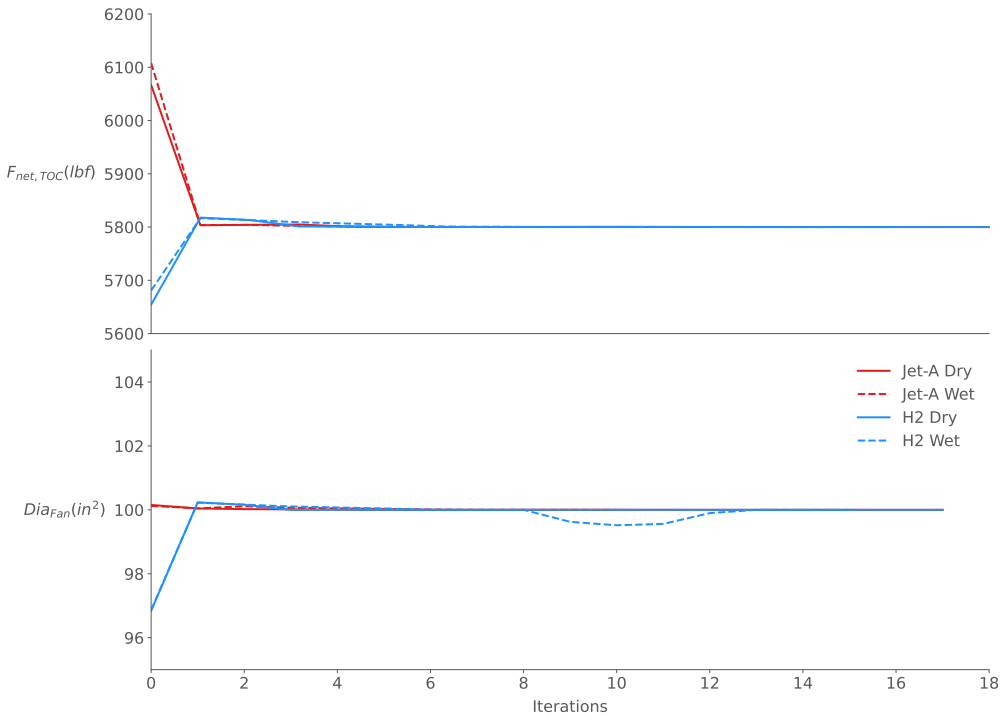

Fig. 10 The constraint history for each optimization problem. Jet-A without water recovery is shown with the solid lines, the Jet-A with water recovery is shown with dashed lines, hydrogen without water recovery is shown with dash-dot lines, and hydrogen with water recovery is shown with dotted lines.

The $T_{4,\text{RTO}}$ value for Jet-A is slightly higher than that of H2. Furthermore, adding water recovery slightly decreases the $T_{4,\text{ratio}}$ value. Therefore, temperatures at cooler with the H2 fuel and barely cooler when adding water recovery. Both fuels have similar efficiencies at the optimal design with Jet-A having a slight advantage in thems of TSEC. Given that most of the design variables change only slightly between designs, most of the efficiency gains are driven by water injection. In fact, we can see the TSEC_{CRZ} improvement due to water recovery relative to no water recovery for both fuels in Figure 12.

Based on this analysis and model, we see an improvement greater than 5% at CRZ for TSEC for both fuels. This level of improvement would have a significant reduction in fuel costs over the course of an engine's lifecycle. Due to the comparatively small amount of water in the exhaust stream for Jet-A, the Jet-A engine would require a larger condenser [3]. This would incure larger condenser mass and pressure penalties compared to the H2 engine which would have more water and requires a smaller fraction of that water. Therefore, H2 is a much more appealing fuel to use with the proposed closed-loop water recovery system. Since no large-scale water condensers have been designed to fit inside a turbofan engine, a relatively low pressure loss condenser would need to be developed for this system to work. Given the lack of knowledge of the type of condenser that would need to be require, we performed a pressure loss sweep of the H2 engine. pyCycle handles pressure losses in ducts by specifyign a pressure loss coefficient, dPqP. This coefficient is the ratio of change in pressure normalized by the inlet pressure of the duct. The pressure loss of the duct just upstream of the extractor was varied while the rest of the engine design variables were optimized. Figure 13 shows TSEC_{CRZ} of this sweep relative to and engine with no water recovery.

From this figure, we can see the design area in which the closed-loop water recovery model is beneficial. This model will offer efficiency benefits up until about dPqP = 0.16 which means a 16% loss of pressure from the condenser. Furthermore, Figure 14 shows the total water available in the core stream as a function of the same pressure loss.

This figure shows that the optimizer finds designs that increase the available water in the core stream. Since the water recovery fraction is always pushed to 17%, the water recovered is increased to overcome the pressure loss. This effect helps the engine increase the benefit area in Figure 13.

The breakdown of thrust for each point is shown in Table 4. This table shows the resulting net thrust, gross thrust, and ram drag of each engine design for the four optimizations performed.

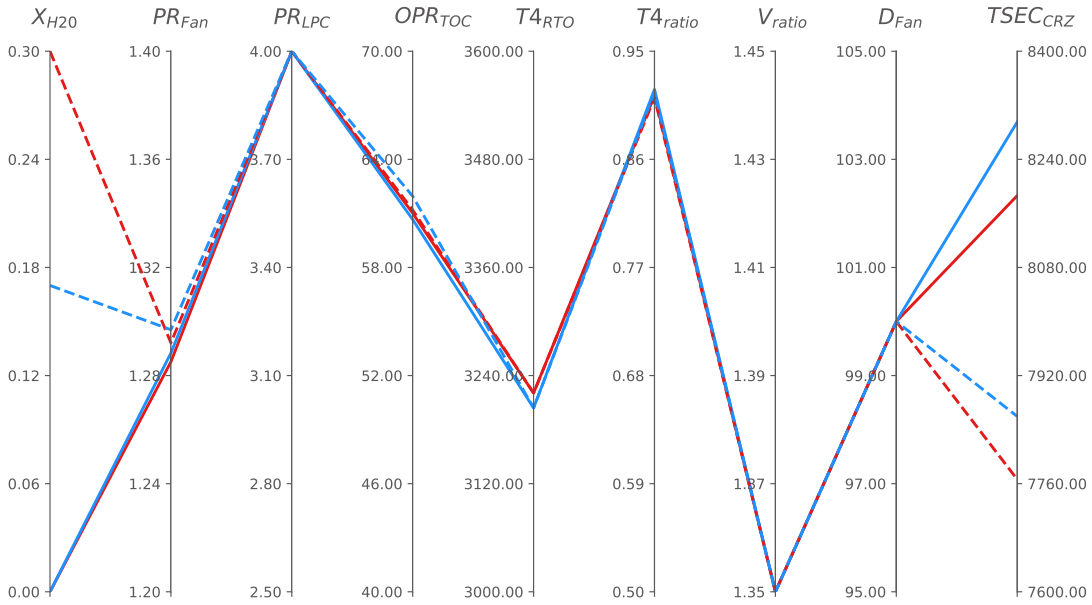

Fig. 11 Optimization results of the N+3 engine with and without no water recovery using Jet-A and H2 as the fuel. The red lines show Jet-A fuel and the blue lines show H2 fuel. The solid lines show the engine without water recovery and the dashed lines show the engine with water recovery.

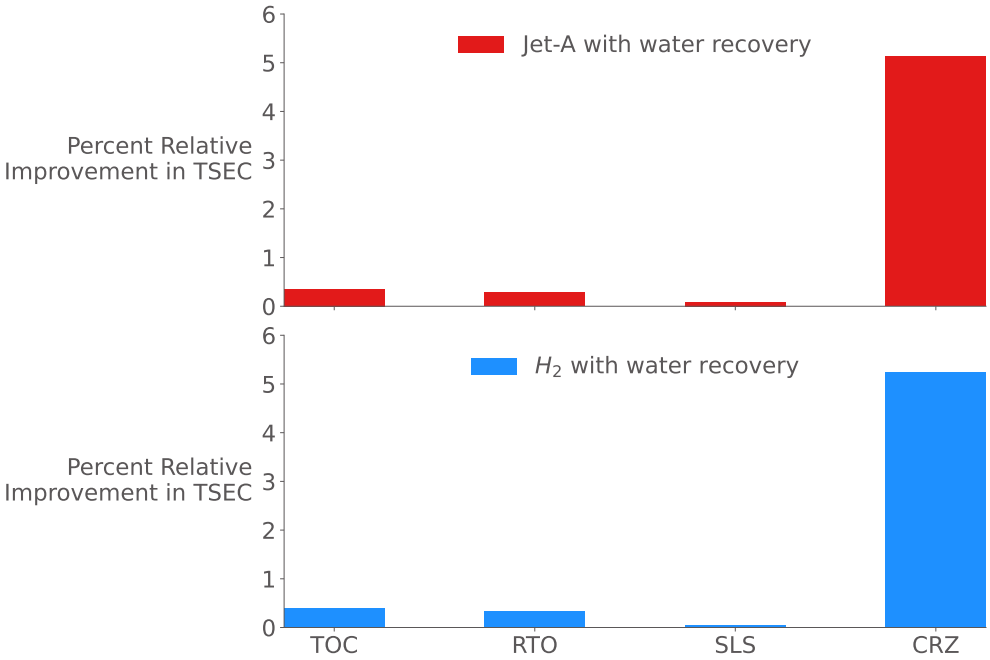

Fig. 12 Percent relative improvement in thrust specific energy consumption (TSEC) of the N+3 engine with water recovery. This plot compares the relative improvement of the two optimziation problems with water recovery compared to the optimzation problems without water recovery.

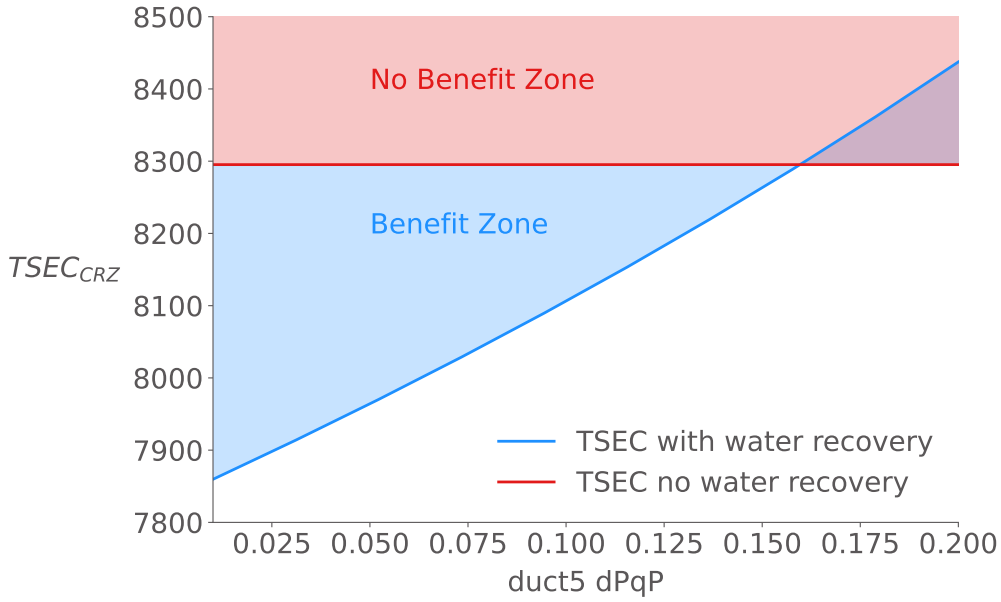

Fig. 13 Pressure loss sweep of Duct5 which is just upstream of the water vapor extractor component. The figure shows the optimized TSEC values for varying levels of pressure loss due to the condensation of water compared to the optimzation problem without water recovery. This shows the working space available for designing a water condensor while still gaining the benefits of water recovery.

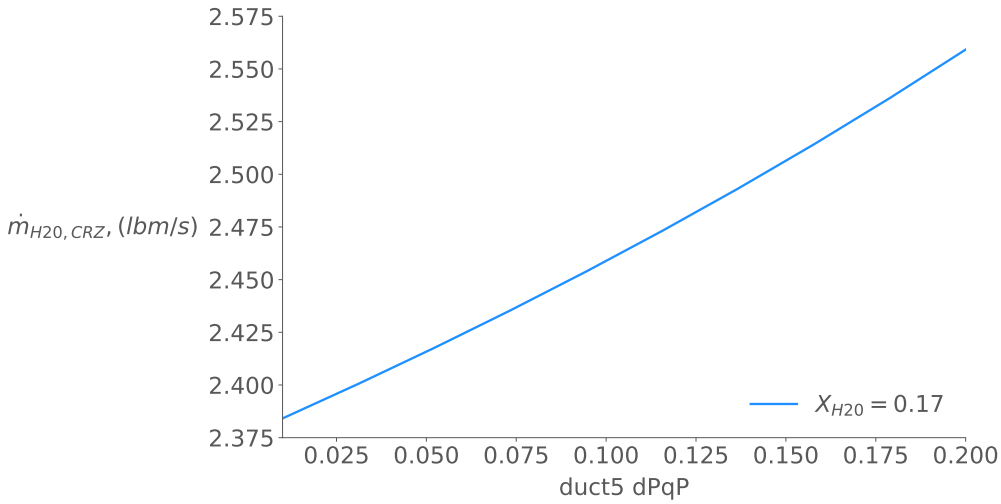

Fig. 14 Pressure loss sweep of Duct5 which is just upstream of the water vapor extractor component. The figure shows the resulting total available water in the exhaust stream for varying levels of pressure loss in the extractor flow path. The engine was optimized with the water recovery upperbound of 17%.

V. Conclusion

VI. Acknowledgements

References

[1] Daggett, D. L., Fucke, L., Hendricks, R. C., and Eames, D. J., "Water Injection on Commercial Aircraft to Reduce Airport Nitrogen Oxides," Tech. rep., NASA, March 2010.

Table 4 Thrust breakdown for each flight operating condition. The net thrust, gross thrust, and ram drag are shown for each optimization result.

Point	Parameter	Jet-A Dry	Jet-A Wet	H2 Dry	H2 Wet
TOC	Net Thrust, lbf	5800.0	5800.0	5800.0	5800.0
	Ram Drag, lbf	19623.4	19623.4	19623.4	19623.4
	Gross Thrust, lbf	25423.4	25423.4	25423.4	25423.4
RTO	Net Thrust, lbf	22800.0	22800.0	22800.0	22800.0
	Ram Drag, lbf	17089.7	17043.5	17070.8	17014.6
	Gross Thrust, lbf	39889.7	39843.5	39870.8	39814.6
SLS	Net Thrust, lbf	28620.8	28620.8	28620.8	28620.8
	Ram Drag, lbf	61.8	61.7	61.8	61.6
	Gross Thrust, lbf	28682.7	28682.5	28682.6	28682.4
CRZ	Net Thrust, lbf	5220.0	5220.0	5220.0	5220.0
	Ram Drag, lbf	19194.0	19152.9	19190.3	19144.1
	Gross Thrust, lbf	24414.0	24372.9	24410.3	24364.1

[2] Mourouzidis, C., Igie, U., Pilidis, P., and Singh, R., "WATER INJECTION ON AIRCRAFT ENGINES: A PERFORMANCE, EMISSIONS AND ECONOMIC STUDY," 2015.

[3] Ström, L. J., and Gierens, K., "First simulations of cryoplane contrails." *Journal of Geophysical Research*, Vol. 107, 2002. doi:10.1029/2001JD000838.

[4] Gordon, S., and McBride, B. J., "Computer Program for Calculation of Complex Chemical Equilibrium Compositions, Rocket Performance, Incident and Reflected Shocks, and Chapman-Jouguet Detonations," *NASA Rept. RP-1311*, 1994.

[5] Jones, S., *An Introduction to Thermodynamic Performance Analysis of Aircraft Gas Turbine Engine Cycles Using the Numerical Propulsion System Simulation Code*, NASA, 2007. TM-2007-214690.

[6] Hendricks, E. S., and Gray, J. S., "pyCycle: A Tool for Efficient Optimization of Gas Turbine Engine Cycles," *Aerospace*, Vol. 6, No. 87, 2019. doi:10.3390/aerospace6080087.

[7] Gray, J. S., Chin, J., Hearn, T., Hendricks, E., Lavelle, T., and Martins, J. R. R. A., "Chemical Equilibrium Analysis with Adjoint Derivatives for Propulsion Cycle Analysis," *Journal of Propulsion and Power*, Vol. 33, No. 5, 2017, pp. 1041–1052. doi:10.2514/1.B36215.

[8] Gray, J. S., Hwang, J. T., Martins, J. R. R. A., Moore, K. T., and Naylor, B. A., "OpenMDAO: An open-source framework for multidisciplinary design, analysis, and optimization," *Structural and Multidisciplinary Optimization*, Vol. 59, No. 4, 2019, pp. 1075–1104. doi:10.1007/s00158-019-02211-z.

[9] Hwang, J. T., and Martins, J. R. R. A., "A computational architecture for coupling heterogeneous numerical models and computing coupled derivatives," *ACM Transactions on Mathematical Software*, Vol. 44, No. 4, 2018, p. Article 37. doi:10.1145/3182393.

[10] Jones, S. M., Haller, W. J., and Tong, M. T., "An N+3 Technology Level Reference Propulsion System," Tech. Rep. NASA/TM—2017-219501, NASA Glenn Research Center, 2017. URL `https://ntrs.nasa.gov/citations/20170005426`.

[11] Kalnay, E., Kanamitsu, M., Kistler, R., Collins, W., Deaven, D., Gandin, L., Iredell, M., Saha, S., White, G., Woollen, J., Zhu, Y., Chelliah, M., Ebisuzaki, W., Higgins, W., Janowiak, J., Mo, K. C., Ropelewski, C., Wang, J., Leetmaa, A., Reynolds, R., Jenne, R., , and Joseph, D., "The NCEP/NCAR 40-Year Reanalysis Project." *Bulletin of the American Meteorological Society*, Vol. 77, 1996, pp. 437–471.

[12] Wu, N., Kenway, G., Mader, C. A., Jasa, J., and Martins, J. R. R. A., "pyOptSparse: A Python framework for large-scale constrained nonlinear optimization of sparse systems," *Journal of Open Source Software*, Vol. 5, No. 54, 2020, p. 2564. doi:10.21105/joss.02564.

[13] Gill, P. E., Murray, W., and Saunders, M. A., "SNOPT: An SQP Algorithm for Large-Scale Constrained Optimization," *SIAM Review*, Vol. 47, No. 1, 2005, pp. 99–131. doi:10.1137/S0036144504446096.